Arabian Journal of Chemistry (2022) **15**, 103629

King Saud University

Arabian Journal of Chemistry

www.ksu.edu.sa
www.sciencedirect.com

ORIGINAL ARTICLE

Potential of *Luffa cylindrica* seed as coagulation-flocculation (CF) agent for the treatment of dye wastewater: Kinetic, mass transfer, optimization and CF adsorption studies

P.C. Nnaji [a,*], V.C. Anadebe [b], I.G. Ezemagu [c,*], O.D Onukwuli [c]

[a] *Department of Chemical Engineering, Michael Okpara University, Umudike, Abia State, Nigeria*
[b] *Department of Chemical Engineering, Alex Ekwueme Federal University Ndufu-Alike, Abakaliki, Ebonyi State, Nigeria*
[c] *Department of Chemical Engineering, Nnamdi Azikiwe University, Awka, Anambra State, Nigeria*

Received 16 October 2021; accepted 6 December 2021
Available online 10 December 2021

KEYWORDS

Dye wastewater;
Luffa cylindrica seed;
Coagulation-flocculation;
Box-Behnken design;
CF adsorption study

Abstract *Background:* In dye-based wastewater decontamination, coagulation-flocculation (CF) induced by *Luffa cylindrica* seed (LCS) was applied.

Methods: The effects of parameters (dosage, pH, stirring/settling time) were investigated using one-factor-at-a-time and Box-Behnken jar test which was designed to optimize the removal of color/total suspended solids (CTSS), chemical oxygen demand (COD) and Chromium VI metal. Proximate and instrumental LCS and post-treatment settled sludge characterization, kinetics, mass transfer and CF adsorption study of the process were investigated.

Significant findings: LCS's proximate composition revealed high crude protein, while its instrumental characterization identified a network of structures with an active surface and a partial crystalline composition. At pH 2, the removal efficiency of CTSS was 99.2% at 1400 mg/L for 30mins, COD was 90.07% at 1400 mg/L for 30mins and at pH 6 chromium was 98.29% at 1800 mg/L for 15mins, these were reported at optimum conditions. Kinetic parameters; rate constant, K_{11}, and half-time coagulation, $\tau_{1/2}$ were determined. The CF adsorption isotherm followed the Freundlich pattern and the kinetic was pseudo-second order. After settling for 300 min, dye removal decreased from the original dye concentration of 1000mgL^{-1} to 3mgL^{-1} due to the rapid mass transfer process. R^2 was > 0.9 for all the studies, and error indicators reported low values. The high dye-polluted wastewater decontamination potential of bio-coagulant was therefore established. The kinetic, mass

* Corresponding authors.
E-mail addresses: pc.nnaji@mouau.edu.ng (P.C. Nnaji), ifegodfey@yahoo.co.uk (I.G. Ezemagu).
Peer review under responsibility of King Saud University.

Production and hosting by Elsevier

https://doi.org/10.1016/j.arabjc.2021.103629

transfer and CF adsorption study data obtained may be useful for bio-coagulation system design, a start-up operating time, design control and optimization.

1. Introduction

Water pollution is a global issue that affects not only humans but the entire biological population. In natural surface water supplies, water contamination can occur unintentionally, carelessly, or unlawfully discharging contaminated wastewater (Nnaji et al., 2020a; Ezemagu et al., 2020b). The increased manufacturing of dye has resulted in the proliferation of industrial wastewater generation from dye-based industries, particularly to meet the increasing population's textile needs. Dye color and heavy metals are the main contaminants in most wastewater. Dye color is due to incompetent manufacturing process in dye-based industries, while heavy metals are the product of their extensive industrial use, especially in fertilizers, paints, batteries, paper, textiles, industries, etc (Onukwuli et al., 2021; Nnaji et al., 2020b). The toxicity and the presence of this color in very small quantities is extremely visible and detrimental to marine life. The decomposition of organic contaminants from dye materials can create toxic compounds that are considered mutagenic. These compounds are not biodegradable due to their high molecular mass and complex molecular structures (de Souza et al., 2016; Hadi et al., 2019). In addition, the structure of certain synthetic dyes has a benzene ring that can be hazardous to human and/or animal life due to their high thermal and long-term stability (Jafari et al., 2020).

Similarly, due to their poor biodegradability, carcinogenicity and bioaccumulation (Wang et al., 2019), the presence of heavy metals in wastewater poses a severe disposal problem. If the wastewater is not properly disposed of in an environment, this heavy metal usually contaminates the soil, food chain, water supplies and air, and this could result in irreparable harm to various organs, tissues, nervous and reproductive systems, even in trace quantities (Wang et al., 2019). One of the heavy metals that present a major environmental issue in dye wastewater is chromium VI. The introduction of Cr (VI) into the environment is primarily due to human activities in the fields of chemicals, electroplating, leather, and textiles. Chromium VI is particularly harmful to animals, humans, and environmentally toxic. Acute nasal septum and respiratory sensitization (asthma), inflammation, and ulceration are caused by inhalation of chromium VI; kidney and liver function are impaired by ingestion and carcinogenic effects have been observed (AWWA, 2012).

A broad variety of technologies based on various decontamination processes, which are known as either biological or physical technology, and advanced oxidation, are used for decontamination of effluents containing dye (Li et al., 2020). These technologies could be ion exchange, membrane isolation, reverse osmosis, precipitation, electrocoagulation, coagulation/co-precipitation, and adsorption etc (Akpomie & Conradie, 2021; Irfan et al., 2017; Nnaji et al., 2020c; Alves et al., 2020). Coagulation-flocculation (CF), a phyco-chemical technological solution stands out as the most feasible primary option for extracting pollutants from wastewater containing dyes, despite all these techniques due to a number of reasons (Menkiti et al., 2015; Okolo et al., 2016).

The CF is the application of coagulant to wastewater to destabilize and neutralize charges that keep the color/colloid in suspension and then aggregate the resulting individual particles(Nnaji et al., 2014; Menkiti & Ezemagu, 2015; Okolo et al., 2016; Ezemagu et al., 2016). The mechanism of CF that relies on the physical and chemical properties of the solution, the contaminants present, and the coagulant type include hydrolysis, coagulation, *peri*-kinetic and orth-kinetic flocculation (Howe et al., 2012). Peri-kinetic and orth-kinetic flocculation is driven by interparticle bridging and sweep flocculation (physical adsorption). The aggregation of particles takes place through this adsorption mechanism.

Essentially, coagulation-flocculation process using bio-coagulant exhibits two principal mechanisms; charge destabilization/neutralization, and interparticle bridging/sweep flocculation. The later occur through adsorption and could be likened to conventional adsorption (Jadhav & Mahajan, 2014; Ezemagu et al., 2020a; Menkiti & Ezemagu, 2015). Coagulation-flocculation are the fundamental processes at most water treatment plants and modern wastewater treatment plants where solid–liquid separation is of considerable significance in practice. It is also widely used to remove color/-colloid dispersion in dye-based wastewaters using various coagulants (Nnaji et al., 2020c).

Chemical coagulants have been widely used to extract a wide variety of pollutants from wastewater. However, the brownish coloring of equipment by iron salt and the post-contamination issues associated with aluminum salts are an inherent drawback (Okolo et al., 2018). Health issues such as Alzheimer's disease in humans (Irfan et al., 2017), generation of large volume of sludge leading to huge disposal cost and inefficiency of aluminum salt in low-temperature waters (Ezemagu et al., 2021a) was reported.

The ability of coagulants from biological origin in reducing the hazards associated with wastewater and the growing concern for environmental issues caused using conventional coagulants, resulted to search for more biological alternative that are ecofriendly. Due to their biodegradability, reusability, wide availability, eco-friendly, easy preparation and efficient performance, natural organic (plant based) coagulants are the most preferred (Ani et al., 2012). Natural bio-coagulants like *Moringa olifera*, tannins, *Detarium microcarpum*, mucuna seed, etc. has been researched on with good results (Okolo et al., 2016; Ani et al., 2012; Nnaji et al., 2020c). Wastewater treated with natural coagulant using processes of CF as opposed to synthetic coagulants does not pose any risk to biological species. The generated sludge can be anaerobically digested and composted to produced biogas and biofertilizer (Ezemagu et al., 2021c; Ejimofor et al., 2021).

Luffa cylindrica seed, the coagulant for the CF process belongs to the cucurbitaceae family. *Luffa cylindrica* seed are

readily found in Senegal, Gambia, Guinea, Serra leone, Liberia, Mali, Ghana, Nigeria etc. *Luffa cylindrica* seed is dispersed pantropically and sub tropically to countries where rainfall is high. Luffa consists primarily of cellulose (60%), hemicellulose (30%), and lignin (10%), and is thus, called lignocellulose (Shahidi et al.,2015). Luffa fresh gourd is used as an edible vegetable, in medical treatment, and the sponge finds wide applications, among others, in packaging, shoe mats, soundproof linings, plant, algae, bacteria, and yeast immobilization matrix (Anastopoulos & Pashalidis, 2020). Luffa consists of protein and carbohydrate; hence can be used a coagulant in decontamination of aqueous effluent (Baharlouei et al., 2018). *Luffa cylindrica* seed's biodegradability, non-toxicity, and healthy nature for human and animals alike, makes it relevance.

However, most of the works on dye-based wastewater decontamination were centered on OFAT (one factor at a time) technique. OFAT consumes time and should not be applied in predicting desired optimum CF efficiency based on the interactions between the process factors (Ezemagu et al., 2021b; Ejimofor et al., 2021a). The process variables that influence CF are temperature, solution pH, wastewater content, coagulant concentration and type, etc. Therefore, optimizing these factors will increase the performance of the process significantly. Response surface methodology (RSM), a set of statistical concepts for the design of model building experiments, the evaluation of the influences of different factors, and the search for the optimal conditions of the variables, was proposed (Onukwuli et al., 2021; Ezemagu et al., 2021a). Box-Behnken design (BBD) is one of the vital components of RSM. Unlike center composite design and other designs in RSM, the BBD consumes less time with few experimental runs and precise results, hence, is usually applied in industrial research (Ezemagu et al., 2021a).

Furthermore, many industrial coagulation-flocculation (CF) processes involving particle agglomeration involve rapid transfer of particle mass and adsorption. Since they are efficient in suspending solid particles, CF processes and most industrial processes use agitated vessels, ensuring that all usable surface area is used, resulting in a good mass transfer rate. Accurately specifying kinetic, mass transfer, optimization and CF adsorption parameters will eliminate or substantially decrease over-design and boost sound control structures by improving the operational efficiency of the unit (Jimoda et al., 2013). Precise equipment size can be assured with the correct parameters, risks can be quantified confidently and optimum operating policies can be adequately defined. There is no documented evidence in the literature on the kinetics, mass transfer, optimization, and CF adsorption studies of the *Luffa cylindrica* seed induced CF process for the decontamination of dye-based wastewater. Therefore, the importance of this work is evident.

Hence, the aim of the present work is to investigate the use of *Luffa cylindrica* seed (LCS) induced CF process for the decontamination of dye-based wastewater. Specifically, this bio-coagulant was used to assess the removal of color/total suspended solids (CTSS), heavy metal, and COD from the wastewater. Physiochemical characterization of *Luffa cylindrica* seeds were gotten. Fourier transfer infrared (FTIR), Scanning electron spectroscopy (SEM)/elemental and X-ray diffraction (XRD) were applied to observe the *Luffa cylindrica* seed (LCS) and the post treated settled sludge after coagulation (PTSS) for its morphological, spectral, elemental composition and crystalline properties. The study's specific objectives also, included coagulation process kinetics, sorption kinetics and isotherm modelling of CF adsorption, mass transfer (coagulation rate-based modelling), and CF process optimization.

2. Experimental section

2.1. Materials, preparation and characterization

At CONRAWS Scientific Equipment Nigeria Limited, the Cibacron blue (3GA) and dispersed red 220 dyes were collected in Enugu, Nigeria. Without further processing the dye materials were applied. Dye-based wastewater was prepared for a 1000mgL^{-1} concentration by dissolving the same ratio of Cibacron blue (CBD) and dispersed red (DRD) in distilled water.

2.1.1. Luffa cylindrica seed (LCS)

Luffa cylindrica sponges were collected around farm settlements in Amawom, Ikwuano Local Government Area, Abia State, Nigeria, between August and September, and dried in sun. The *Luffa cylindrica* seeds were isolated from the matured dried sponges. Separated seeds were washed, dried and homogenized to obtain LCS and placed in an airtight container for further use (see Fig. 1). The proximate analysis of the LCS was based on standard methods (AOAC, 2005). Coagulant (LCS) and post treatment settled sludge (PTSS) were characterized using the following instruments: an infrared spectrometer (Agilent Technologies) with a resolution range of 4000–650 cm^{-1} and 30 8 cm^{-1} scans with 16 background scans to obtain FT-IR spectra. A scanning electron microscope (Phenon-World, MVE 016477830) for morphological characteristics of the sample. An X-Ray diffractometer (XRD) spectrum was obtained using PHILIPS – ASCII (UDF) with XPERT diffractometer to determine the crystalline nature of the materials.

2.1.2. Dye-based wastewater

The characterization of dye-based wastewater was determined by standard methods (AWWA, 2012). The COD and the Cr (VI) were determined using dichromate method (5220A) and flame adsorption spectrophotometry (3111B), respectively (AWWA, 2012).The characterization was carried out at the National Soil, Plant, Fertilizer, and Water Laboratory, Umudike, Nigeria. Mettler Toledo Delta 320 pH meter, Conductivity meter, DDS 307 and UNICO 1100 Spectrophotometer were used to evaluate the pH, electrical conductivity and CTSS.

2.2. Coagulation-flocculation (CF) test (Jar test)

The CF process was carried out utilizing a jar test approach, in which LCS (with concentration 1.0–1.8gL^{-1}) was added to 200 mL of wastewater at various pH values (2–10). Sulphuric acid and sodium hydroxide, both at 0.1 M, were used to achieve pH adjustment between 2 and 10. It was decided to undertake 5mins quick stirring at 150 rpm followed by 30 min of gentle stirring at 25 rpm. The coagulant was applied before the agitation. After 30 min of slow stirring, the solution was gently put into a 250 mL cylinder and allowed to settle. A UV–VIS spectrophotometer (UNICO 1100, with wavelength

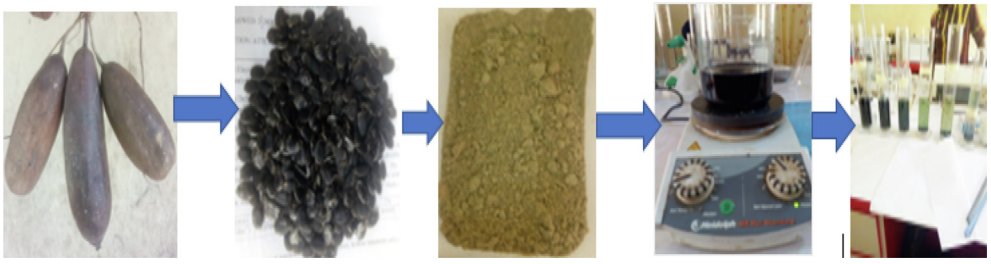

Fig. 1 Schematic diagram of LCS preparation up to application as coagulant.

range 330–900 nm and sample cell length of 10 mm) was used to measure the absorbance of a 10 mL supernatant pipetted 2 cm below the solution at various time intervals.

2.3. Determination of CTSS, COD and chromium (VI) metal removal

Using the direct proportionality between absorbance and concentration, the percentage CTSS removal from dye-based wastewater was determined. The initial absorbance was reported before the process of CF was carried out and the absorbance at each time was recorded. From this, the percentage CTSS removal for each of the coagulant dosages was calculated. The supernatant obtained after the CF process was analyzed with a standard method according to AWWA (2012) for COD and chromium (VI) content.

*2.4. **Coagulation-flocculation (CF) kinetic principles***

The clusters-size distribution of colloidal particles as time evolves is described by the Smolunchowski as (Okolo et al., 2016):

$$\frac{dN_n}{dt} = \frac{1}{2}\sum_{j=n-i} K_{ij}N_iN_j - N_n\sum_{i=1}^{\infty} K_{in}N_i \tag{1}$$

Where, $N_n(t)$ is the time-dependent number concentration of n-fold clusters, t is the time, and K_{ij} are the elements of the rate kernel which control the rate of coagulation between an i-fold and an j-fold cluster. However, from Smolunchowski approximation, the coagulation is entirely controlled by Brownian diffusion and the coagulation rate constant for dimmer formation of an initially mono-disperse suspension is then given by:

$$K_{11} = \frac{8K_BT}{3\eta} \tag{2}$$

where K_B is the Boltzmann constant, T is the absolute temperature, and η is the medium viscosity. It has been reported that for a constant kernel, i.e., $K_{ij} = K_{II}$, the Smolunchowski Eq. (1) can be resolved to obtain the expression:

$$\frac{N_n(t)}{N_0} = \frac{(K_{11}N_0t/2)^{n-1}}{(1+K_{11}N_0t/2)^{n+1}} \tag{3}$$

where N_o is the initial particle concentration.

From Eq. (3), the linear functions in time for the inverse square root of monomer concentration N_1 is given by the expression:

$$\frac{1}{\sqrt{N_1}} = \frac{1}{\sqrt{N_0}}\left(1+\frac{K_{11}N_0t}{2}\right) \tag{4}$$

From Eq. (4), $\frac{1}{\sqrt{N_1}}$ vs t can be plotted and fitted using MATLAB 2015a software. The linear polynomial model F (x) = P_1 * X + P_2 similar to Eq. (4) was used for the fit. The coagulation rate constant can be evaluated from the slope. Also, the rapid coagulation rate constant, $K_R$is given by Smoluchowski as:

$$K_R = \frac{4K_BT}{3\eta} \tag{5}$$

Combination of Eqs. (2) and (5) gives:

$$K_R = 1/2K_{11} \tag{6}$$

Furthermore, the coagulation time or the time when the total number concentration of particle is reduced by a factor of 2 is obtained using Eq. (7).

$$\tau_{1/2} = \frac{2}{K_{11}N_0} \tag{7}$$

This coagulation time represents a useful time scale for the identification of the early stages in the CF process. Denoting the number of concentrations of n-fold aggregates at reduced time as $\tau_{1/2}$.

Absorbance is converted to suspended solid particles concentration (N), mgL^{-1}, using Beer's law as shown.

$$A = \varepsilon mCL \tag{8}$$

Where A = Absorbance, εm = molar extinction coefficient, C = concentration, L = path length of 1 cm

$$\text{CTSSremoval} = N_0 - N_n \tag{9}$$

N_o = Initial Particle Concentration and N_n = Particle Concentration at time, t.

2.5. CF adsorption isotherm and kinetic modeling

The sorption mechanism, inter particle bridging, and sweep flocculation cause floc development in coagulation-flocculation, which can be reproduced as an adsorption phenomenon (Jadhav & Mahajan, 2014; Ezemagu et al., 2020). To determine the CF adsorption effectiveness of LCS in the CF process, the data obtained from the jar test experiment was used to model the isotherm using Langmuir, Freundlich, and Temkin models, as well as adsorption kinetics using Lagergren pseudo first order and Ho's pseudo second order models.

2.5.1. Langmuir isotherm

The Langmuir isotherm is based on the fact that the maximal adsorption on the adsorbent surface corresponds to a saturated monolayer of solvent molecules, the adsorption energy is uniform, and no adsorbate transmigration on the surface plane ((Ezemagu et al., 2016). The Langmuir equation is written as:

$$\frac{1}{q_e} = \frac{1}{q_m} + \left(\frac{1}{K_l q_m}\right)\left(\frac{1}{C_e}\right) \tag{10}$$

Where $K_{L,}$ is the Langmuir constant (Lg^{-1}); q_e is the equilibrium dye concentration on the adsorbent (gg^{-1}); C_e is the equilibrium dye concentration in solution (gL^{-1}); qm is the concentration of dye when the adsorbent forms a monolayer (gg^{-1}). K_L and q_m can be evaluated from the slope and intercept of plot $\frac{1}{q_e} vs \frac{1}{C_e}$.

2.5.2. Freundlich isotherm

The Freundlich isotherm is based on the premise that biosorption heat has a heterogeneous surface with a non-uniform distribution over the surface. The linearized empirical equation is expressed as:

$$lnq_e = lnK_f + 1/nlnC_e \tag{11}$$

Where the Freundlich constant is $K_f(gg^{-1}L^{1/n}\,g^{-1/n})$ and 1/n is the heterogeneity factor associated with the bio-sorption potential and strength, respectively.

2.5.3. Tempkin isotherm

The Tempkin isotherm model considered the impact on adsorption isotherms of certain indirect adsorbate/adsorbate interactions and proposed that the adsorption heat of all the molecules in the layer would decrease linearly with coverage due to these interactions (Menkiti et al., 2018). The Tempkin isotherm linearized equation is given as:

$$q_e = BlnA + BlnC_e \tag{12}$$

2.5.4. Adsorption kinetics

To determine the mechanism of **CF adsorption performance** on the biomass during the **CF** process, the Lagergren pseudo first order model, Ho's pseudo second order model, was analyzed. The expression for pseudo first order rate is given as:

$$log(q_e - q_t) = \log(q_e) - K_1 \frac{t}{2.303} \tag{13}$$

The rate constant of first order adsorption (min^{-1}) is $K_{1,}$ where q_e and q_t are the amount of dye adsorption on biomass at equilibrium and at time t, (gg^{-1}), respectively. The rate of pseudo second order is expressed by (Menkiti et al., 2018):

$$\frac{t}{q_t} = \frac{1}{(K_2 q_e^2)} + \frac{t}{q_e} \tag{14}$$

Where the rate constant K_2 is for pseudo second order adsorption ($gg^{-1}min^{-1}$).

2.6. *Coagulation-flocculation diffusion model formulation*

From counter-current and simultaneous diffusion of particles from dense to less dense particle regions, a mathematical model explaining the transfer rate of mass (coagulated particles) in the wastewater treatment during CF process was created, as shown in Fig. 2a. By defining the simplifying assumptions, identifying the correct initial and boundary conditions of the process, the conservation of particle mass in the wastewater treatment system for CF was achieved. The following assumptions have been made: wastewater homogeneity and one-dimensional mass transfer in the process. The initial wastewater particle concentration is uniform and the internal resistance to the movement of particles was overlooked.

Considering conservation of mass of particles in the coagulation-flocculation system as illustrated in Fig. 2b, we will have:

Time rate of change of mass in the system

$$= \textit{influx of mass into the system} - \textit{outflux of mass from the system} \tag{15}$$

$$\text{Time rate of change of mass in the system} = \frac{\partial (C) Ax}{\partial t} \tag{16}$$

$$\text{Influx of mass into the system} = j \tag{17}$$

$$\text{Outflux of mass from the system} = j + \frac{\partial j}{\partial x} Ax \tag{18}$$

Where C = concentration, j = flux of the mass per unit time, A = area, x = characteristic length (m), and t = time.

Applying Eqs. (16) to (18) in Eq. (15), we have:

$$\frac{\partial (C) Ax}{\partial t} = -\left(+\frac{\partial j}{\partial x} Ax\right) \tag{19}$$

Divide Eq. (19) by Ax gives;

$$\frac{\partial c}{\partial t} = -\frac{\partial j}{\partial x} \tag{20}$$

Recalling, Fick's first law:

$$J = -D_{eff} \frac{\partial C}{\partial x} \tag{21}$$

D_{eff} = Effective diffusion coefficient

And then, combining Eqs. (20) and (21), gives:

$$\frac{\partial C}{\partial t} = \frac{\partial}{\partial x}\left(D_{eff} \frac{\partial C}{\partial x}\right) \tag{22}$$

Eq. (22) is a partial differential equation which describes the rate of mass transfer during the CF of wastewater using biomass. Using Eq (23), D_{eff} was computed for an effective particle diffusion coefficient. (Menkiti & Onukwuli, 2011)

$$K_R = 8\pi r D \tag{23}$$

2.6.1. Numerical solution technique (finite difference technique)

With a view to solving the Eq. (22), the technique of approximation was used. The explicit finite difference method (FDM) was applied and the equation was transformed into a differential equation by dividing the solution domain into a grid of points represented along with each mesh point and referred to as nodes in the form of mesh and derivatives. The solution was obtained when at each node the dependent variable was first defined, and then approximated until the final step for

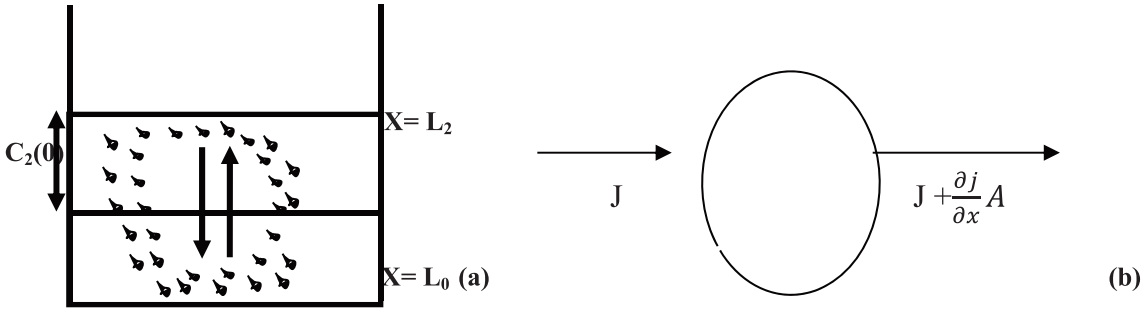

Fig. 2 Schematic outlay of the process showing L_2, height of coagulated wastewater, the interface of less and rich-particle zones(a), Species conservation in CF (b).

the next step. Therefore, the finite display of the mesh points is shown as follows (Jimoda et al., 2013):

$$Xi = i\delta x, \ for \ i = 0, 1, 2 \cdots\cdots\cdots .m \tag{24}$$

$$Yj = j\delta t, \ for \ j = 0, 1, 2 \cdots\cdots\cdots .n \tag{25}$$

Where δx and δt indicate grid sizes and subscripts denote the location of the dependent variable being considered in the × and t directions, respectively. Let the process of jar **CF** occupy the $0 \leq x \leq L$ space and divide the gap in the space of the unit into equal δx intervals and time into δt intervals. The finite difference representations of various derivatives appearing in the governing equation are obtained from expanding the Taylor series (Stroud, 1987). Then, applying the expansion in the t-direction while preserving the constant and truncated second term of the series for the left side of Eq. (22) then gives,

$$C_{i,j+1} = C_{i,j} + \delta t(\frac{\partial C}{\partial t})_{i,j} \tag{26}$$

$$\frac{C_{i,j+1} - C_{i,j}}{\delta t} = (\frac{\partial C}{\partial t})_{i,j} \tag{27}$$

Therefore,

$$\frac{\partial c}{\partial t} = \frac{C_{i,j+1} - C_{i,j}}{\delta t} \tag{28}$$

Similarly, expanding in the x-direction, keeping t, constant, i.e., for the right-hand side of Eq. (22), becomes:

$$C_{i+1,j} = C_{i,j} + \delta x(\frac{\partial C}{\partial x})_{i,j} + \frac{(\partial x)^2}{2}\frac{\partial^2 C}{\partial x^2} \tag{29}$$

Again, applying Taylor's series expansion in × direction (backward difference) keeping t constant:

$$C_{i-1,j} = C_{i,j} - \delta x(\frac{\partial C}{\partial x})_{i,j} + \frac{(\partial x)^2}{2}(\frac{\partial^2 C}{\partial x^2}) \tag{30}$$

Adding Eqs. (29) and (30) gives:

$$\frac{\partial^2 c}{\partial x^2} = \frac{C_{i,-1} - 2C_{i,j+}C_{i+1,j}}{(\delta x)^2} \tag{31}$$

Equating Eq. (28) to Eq. (31) and introducing D_{eff} as in Eq. (22) gives the governing equations:

$$\frac{C_{i,j+1} - C_{i,j}}{\delta t} = D_{eff}\frac{C_{i,-1j} - 2C_{i,j+}C_{i+1,j}}{(\delta x)^2} \tag{32}$$

$$C_{i,j+1} - C_{i,j} = D_{eff}\frac{\delta t}{(\delta x)^2}C_{i-1,j} - 2C_{i,j+}C_{i+1,j}$$

$$C_{i+1,j} = C_{i,j} + r\left[C_{i-1,j} - 2C_{i,j} + C_{i+1,j}\right] \tag{33}$$

Where r $= \frac{D_{eff}\delta t}{(\delta x)^2}$

At

$$x = 0, then, i = 0, \ hence, \ C_{0,j+1} = C_{0,j} + r\left[C_{-1,j} - 2C_{0,j} + C_{+1,j}\right] \tag{34}$$

Then, calculate $C_{-1,j}$ (pseudo concentration at external mesh point) and depicts the relevant grid points at x = 0 and x = L. The simplest way to represent the condition at x = 0, for forward difference, in finite difference is given by:

$$\frac{C_{1,j} - C_{0,j}}{\delta x} = C_{0,j}$$

This gives an additional $C_{0,j}$ equation at any time stage to be used instead of a given $C_{0,j}$ value in an explicit finite difference. Now, $C_{-1,j}$ must be inserted at the external mesh point to represent a pseudo concentration more accurately at × = 0 by the central difference equation by imagining that the tissue sheet is very slightly extended. Accordingly, in terms of central difference representation, the finite difference approximation at boundary x = 0 is:

$$\frac{C_{1,j} - C_{-1,j}}{2\delta x} = C_{0,j} \tag{35}$$

To eliminate $C_{-1,j}$ between Eqs. (33) and (34), we have that Eq. (35) as:

$$C_{-1,j} = C_{1,j} - 2\delta x C_{0,j} \tag{36}$$

Substitute Eq. (36) into Eq. (34) and expanding gives

$$C_{0,j+1} = C_{0,j} + r\left[C_{1,j} - 2\delta x C_{0j} - 2C_{0,j} + C_{1,j}\right]$$

$$C_{0,j+1} = C_{0,j} + 2r\left[C_{1,j} - C_{0j}(1 + \delta x)\right] \tag{37}$$

Similarly, at × = L (for other side of the tissue) the derivative boundary condition becomes:

$$C_{10,j+1} = C_{10,j} + 2r\left[C_{9,j} - 2C_{10j} + C_{11,j}\right] \tag{38}$$

In terms of central difference representation, we have,

$$\frac{C_{11,j} - C_{9,j}}{2\delta x} = C_{10,j} \tag{39}$$

Similarly, if the value (C_{11}) is eliminated between Eq. (38) and Eq. (39), we have:

$$C_{10,j+1} = C_{10,j} + 2r\left[C_{9,j} - (1+\delta x)C_{10,j}\right] \quad (40)$$

2.6.2. Computer programming and simulation

Codes for Eq. (40) implementation for the rate of mass transfer during wastewater coagulation using LSC was developed in the MATLAB environment and analyzed under various process operating conditions. The criterion for the stability and convergence of the solution was tested and met ($\frac{D_{eff}\delta t}{\delta x} \leq \frac{1}{2}$) for each simulation run of the CF process. The following statistical parameters were used: mean square error (MSE), root mean square error (RMSE), mean absolute percentage error (MAPE), and mean absolute deviation (MAD). Using Eqs (41) – (44)., the statistical parameters above were calculated.

$$MSE = \frac{\sum_{t=1}^{n}(A_t - F_t)}{n} \quad (41)$$

$$RMSE = \sqrt{\frac{\sum_{t=1}^{n}(A_t - F_t)^2}{n}} \quad (42)$$

$$MAPE = \frac{\sum_{t=1}^{n}\left|\frac{A_t - F_t}{A_t}\right|}{n} \times 100 \quad (43)$$

$$MAD = \frac{\sum_{n}^{t=1}|A_t - F_t|}{n} \quad (44)$$

2.7. Box-Behnken design (BBD) of experiment

In the design of the RSM jar test, BBD implementing RSM from Design Expert 10.0 portable was used. BBD is a three-level architecture for quantitative variables for all variables. The architecture has varied across three levels for each of the numerical factors; high (+1), low (-1) and middle (0). The experiment required a total of 17 runs (Table 1). The response variables (Y %) were %CTSS, %COD and %Cr (VI) removal, while, LCS dosage (X_1), solution pH (X_2) and stirring time (X_3) were the independent variables affecting the response variables (Y%). The spectrum and levels used in the analysis are indicated in Table 1. This method is intended to suit the quadratic polynomial equation (Kim, 2016; Ahmadi et al., 2016; Ezemagu et al., 2021) of this model form:

$$y = b_o + \sum_{i=1}^{k} b_i X_i + \sum_{i=1}^{k} b_{ii} X_i^2 + \sum_{i}^{k}\sum_{j} b_{ij} X_i X_j \quad (45)$$

The independent variables affecting y, b_o, b_i, b_{ii} and b_{ij} are the offset terms, ith linear coefficient,

iith quadratic coefficient and the ijth interaction coefficient where y is the response variable to be modeled; Xi and Xj.

For three variable inputs of X_1, X_2, and X_3, the quadratic response is shown in Eq (46) (Prabhu et al., 2020):

$$Y = b_0 + b_1X_1 + b_2X_2 + b_3X_3 + b_{12}X_1X_2 + b_{13}X_1X_3 + b_{23}X_2X_3 + b_{11}X_1^2 + b_{22}X_2^2 + b_{33}X_3^2 \quad (46)$$

Where Y: response; X_1, X_2, and X_3: autonomous parameters; b_0: constant, b_1, b_2 and b_3: constants were reflecting the influence of parameters X_1, X_2, and X_3; b_{12}, b_{13} and b_{23}: constants were reflecting the interaction between two parameters; and b_{11}, b_{22} and b_{33}: constants were reflecting the quadratic effect.

3. Results and discussion

3.1. Characterization results

3.1.1. *Luffa cylindrica* seed (LCS)

The proximate composition of LCS previously documented (Nnaji et al., 2020b; Onukwuli et al., 2021), revealed 21.88% crude protein, which is high and comparable to published work as one of the active component for CF process. The relative high protein could be the reason for good performance of LCS as a coagulant for the treatment of dye-based wastewater. Documented literature has defatted LCS crude protein ranging from 42.17 to 70.65%, 45.06– 50.06%, whereas non-defatted LCS crude protein is 28.45% (Nnaji et al., 2020b).

3.1.2. Characterization of dye-based wastewater

The characteristics of dye-based wastewater revealed high dissolved solid particles with obvious high conductivity and the presence of heavy metals. The results indicated pH of 5.55, turbidity 340.53FAU, BOD 316.35 mg/L, COD 1930.4 mg/L, Lead 2.27 mg/L, Nickel 8.54 mg/L and Chromium 2.315 mg/L. The value of turbidity shows the presence of total dissolved and suspended solid in the wastewater. The high COD value and the presence of heavy metals such as Lead, Nickel and chromium are indicators of pollution.

3.1.3. FT-IR spectra characterization of LCS and PTSS

It is important to understand the essence and properties of a material in order to make the best use of it. Therefore, FT-IR was used to investigate the LCS and PTSS surface characteristics. The LCS and PTSS spectra are shown in Fig. 3. Fig. 3 showed the existence for LCS and PTSS of a polymer –OH, functional group extending between 3276.3 cm^{-1} and 3280.1 cm^{-1} (Jiang et al., 2020). Methyl C-H and methylene C = H asymmetric stretching is applied to spectra stretch 2951.1–2914.8 cm^{-1} for LCS and PTSS, while 1707.1 cm^{-1} could be carboxylic ketone stretching. For LCS and PTSS, 1636.3 cm^{-1}, 1543.1 cm^{-1}, and 1408.8 cm^{-1} could be due to olefin, aromatic ring stretches and asymmetric alcohol bends, respectively. Similarly, the stretch for LCS and PTSS at 1226.3 cm^{-1} and 1036.2 cm^{-1} may be attributed respectively to skeletal C = C vibration and primary amine C-N The medium peak for PTSS at 1770.5 cm^{-1} and 1457.4 cm^{-1} could be due respectively to carboxylic and skeletal C-C stretching of vibration. Also present in PTSS are 1080.9–1028.7 cm^{-1} stretching and 752.9 cm^{-1} stretching, respectively, which may be cyclohexane vibration and C-H alkyne bend. Protein and fatty acid structures commonly contain these groups, especially the hydroxyl and carboxyl groups (Dalvand et al., 2016). The spectra are comparable to the spectra obtained for organic compounds like protein(Nandiyanto et al., 2019). The majority of the functional groups found in LCS and PTSS serves as an active site for color/colloidal particle attachment

Table 1 BBD for CTSS, COD and Cr (VI) removal from wastewater.

Run	Coded			Uncoded			Responses		
	X_1	X_2	X_3	Dosage (gL^{-1})	pH	Stirring time (mins)	CTSS Removal (%)	COD Removal (%)	Cr(VI) Removal (%)
1.	0	0	0	1.4	6	15.0	58.4	76.97	70.01
2.	−1	0	−1	1.0	6	5.0	56.6	67.48	92.92
3.	1	−1	0	1.8	2	15.0	97.8	88.03	48.62
4.	0	−1	−1	1.4	2	5.0	97.9	87.10	32.48
5.	0	1	−1	1.4	10	5.0	27.0	76.80	46.23
6.	−1	0	1	1.0	6	30.0	35.2	43.34	87.53
7.	−1	1	0	1.0	10	15.0	28.6	67.61	50.78
8.	1	0	−1	1.8	6	5.0	49.0	86.80	89.48
9.	−1	−1	0	1.0	2	15.0	89.4	86.59	44.06
10.	0	0	0	1.0	6	15.0	58.2	76.44	71.42
11.	0	0	0	1.4	6	15.0	58.7	77.89	70.98
12.	0	0	0	1.4	6	15.0	58.4	77.01	72.22
13.	0	0	0	1.4	6	15.0	56.7	77.44	73.58
14.	0	1	1	1.4	10	30.0	29.0	45.30	45.97
15.	0	−1	1	1.4	2	30.0	99.2	90.07	49.02
16.	1	1	0	1.8	10	25.0	35.0	68.93	56.02
17.	1	0	1	1.8	6	30.0	68.4	79.8	98.29

(de Souza et al., 2016; Onukwuli et al., 2021). Another indicator of LCS ability to pick up metal ions in solution is the presence of – OH (which could be proof for possible pore hydration) and carboxylic stretching. The changes in FTIR spectra in the two samples indicate that functional groups are involved in dye and colloidal adsorption during coagulation and flocculation (Joshi et al., 2020). The shift in peaks could be attributed to changes in functional groups' chemical

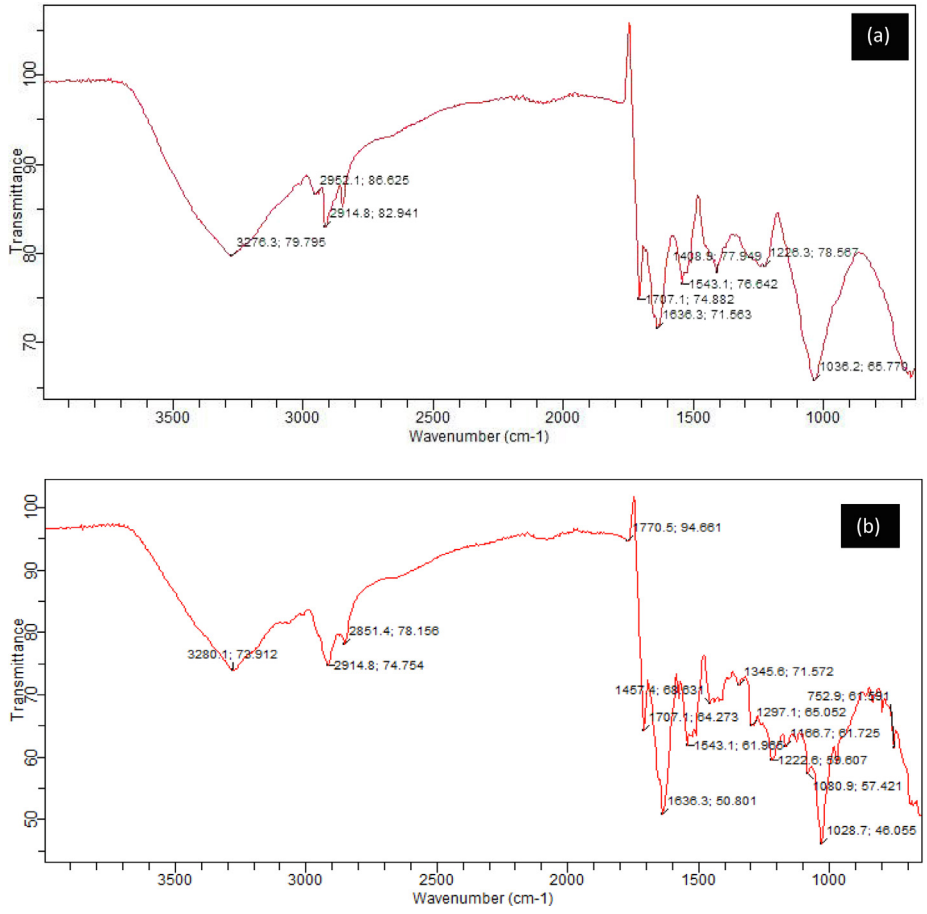

Fig. 3 FTIR spectra of (LCS) (a); Post treatment settled sludge (PTSS) (b).

environment, while, bandwidths appearance and disappearance as seen in PTSS points at reactions that involves the relevant functional groups(Nnaji et al., 2020b).

3.1.4. SEM/elemental results of LCS and SS

LCS and PTSS (post CF) surface morphology is provided in 1500 × magnification (see Fig. 4). Fig. 4a for LCS indicates fibrous nature and irregular structure, some fissures and pores are present. This is an example of a macroporous structure providing active sites for coagulation-flocculation and adsorption (Ahmad & Haseeb, 2015). The PTSS surface morphology displayed in Fig. 4b is in 1500 × magnification. The figure showed expansion of LCS molecules and aggregated particles of LCS and dye, attributed to the CF process involving certain chemical reactions, which led to the breakdown of the existing structure to allow floc formation. Table 2 describes the elemental compositions of LCS, CBD, DRD and PTSS. Clearly, the presence of elements, which were originally not seen in LCS, but subsequently appeared in the PTSS matrix was an indicator of the transfer of elemental particles from dye-based wastewater. The presence or absence of such particles could not be unconnected to a chemical reaction that contributed to depositing or adding the elements to the PTSS matrix, or dissolving them into decontaminated wastewater solution.

3.1.5. XRD results of LCS and PTSS

X-ray diffraction is a valuable method for the study of the material's crystalline structure. Fig. 5 displays the X-ray diffraction spectra for both LCS and PTSS. Fig. 4a for LCS shows 14 clear and high peaks and numerous halos with amorphous humps and lots of noise, while, Fig. 5b indicated 13 clear peaks, between $10 < 2\theta < 70°$ strip. This indicates characteristic patterns of a partially crystalline nature where scattered bands were formed by poorly organized molecules. For PTSS, Fig. 5b showed similarly organized molecules with peak changes. Also, the crystal peaks in Fig. 5 a, b, when compared with the regular crystal peaks shifted from left to right axes, which could be attributed to the expansion or contraction of LCS (Menkiti et al., 2016). Fig. 5a, b indicated crude lattice structure for LCS and PTSS, respectively. The peak changes may be due to reactions that lead to molecular particle attachment. It could be formation of magnesium compound which dissolved into the solution of the treated wastewater. If material studied indicates well defined peaks, it is said to be crystalline, whereas non-crystalline or amorphous material displays halos or humps(Zhao et al., 2017).

3.2. Process factors influence

3.2.1. Effect of LCS on CTSS, COD and chromium (VI) removal

Fig. 6 shows the effect of varying dosages of LCS between 1.0 and 1.8gL^{-1} for the efficiency of CTSS, COD and Cr (VI) removal at varying pH after 300 min settling. Fig. 6a clearly showed better coagulant performance in removing CTSS at acidic medium, especially pH 2, recording > 94% between 1.0

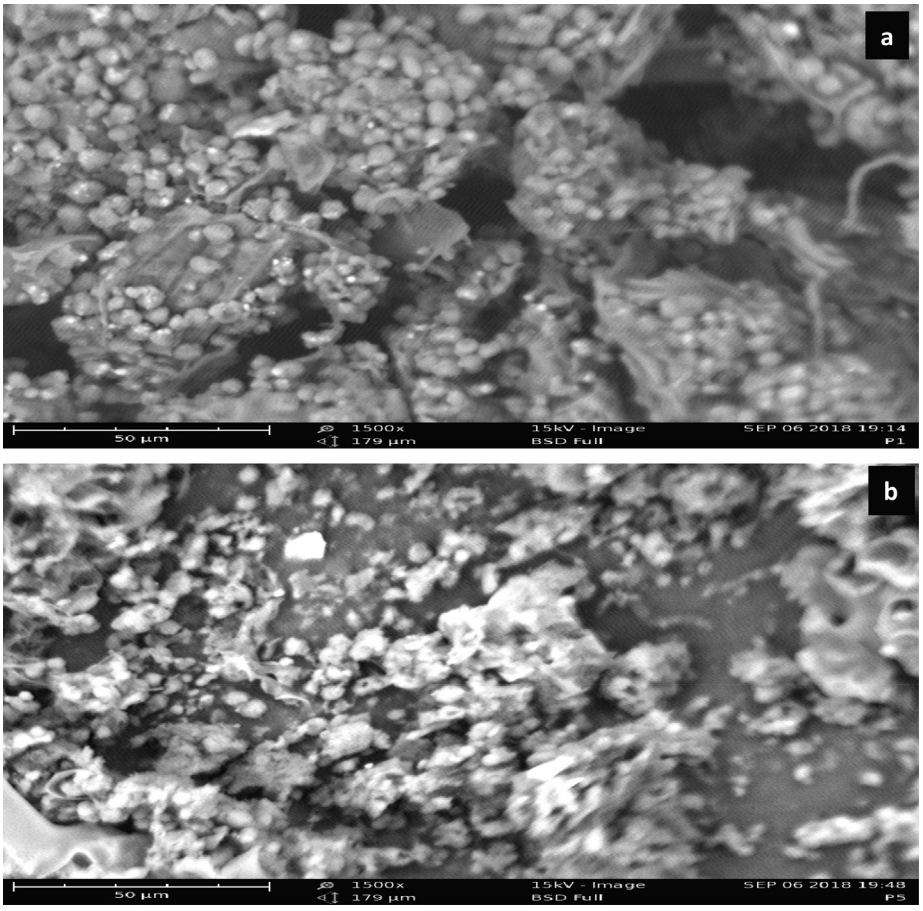

Fig. 4 SEM micrograph LCS at 1500x magnification (a) and PTSS at 1500 × magnification (b).

Table 2 Elemental composition of LCS, dye materials (CBD & DRD) and PTSS.

Element, (wt. %)	LCS	CBD	DRD	SS
Mg	24.10	0.00	4.40	0.00
Al	1.40	1.10	0.60	8.70
Si	1.10	1.20	0.20	15.70
P	34.00	0.23	0.60	22.00
S	9.90	80.9	64.80	33.00
Cl	0.30	3.20	28.80	12.40
Ca	0.60	5.10	0.10	5.40
Ti	0.40	0.30	0.08	1.10
Cr	0.00	1.10	0.00	0.40
Mn	0.07	1.10	0.00	0.00
Fe	1.30	4.10	0.30	1.70
Ni	0.00	0.07	0.00	0.06
Cu	0.06	0.20	0.00	0.00
Zn	0.30	0.04	0.00	0.01
Br	0.00	0.50	0.01	0.00
Sn	26.50	0.00	0.00	0.00
Pb	0.00	0.80	0.00	0.30

and 1.6gL^{-1}. The optimum dosage, however, which provided 98.4% CTSS removal was 1.2gL^{-1} at pH 2. The high efficiency of removal of CTSS could be attributed to the strong interaction between LCS and wastewater molecules that led to the destabilization/neutralization of the negatively charged CTSS particles in dye-based wastewater (Okolo et al., 2016). The lower efficiency of removal recorded at other pH, in particular, pH 4 to 8 could be linked to reversal of the charges on particles resulting in re-stabilization and a decline in CF. LCS was believed to have functional groups which serve as an active site for CTSS attachment(Ani et al., 2012). Fig. 6b shows the COD removal efficiency at varying pH and biomass dosage after 300 min of settling. Fig. 6b clearly highlighted better biomass performance at pH 2, which recorded between 86.53 and 88% for all dosages. This can be due to a reduction of the wastewater organic portion (CTSS) prior to the COD test. Acidic medium performance is compatible with other literatures, as it favors the oxidation reaction that resulted in the removal of organic wastewater components (Jorfi et al., 2018). The optimum dosage of 1.4gL^{-1} at pH 2 gives the best COD removal efficiency of 88%. Fig. 6c shows the effect of varying dosage of coagulant between 1.0 and 1.8gL^{-1} and pH between 2 and 10 for removal efficiency of chromium (VI) after 300 min settling time. Fig. 6c shows a different impact on coagulant efficiency when removing chromium (VI) from dye-based wastewater compared with CTSS and removal of COD. The figure indicated better output at an aqueous pH 6–10 for all dosages applied. As the dosage increases, the removal of chromium (VI) increased, but undeniably the lowest was reported at pH 2. The best coagulant performance for removal of chromium (VI) was reported at pH 6 with 1.8gL^{-1} providing a removal efficiency of 97.5%. The active attachment site established in LCS could be attributed to this performance.

3.2.2. Effect of settling time on CTSS removal using LCS

The effect of settling time on removing CTSS using LCS was assessed at varying wastewater pH and dosage of 2 – 10 and 1.0 – 1.8gL^{-1}, respectively, in the range 5 – 300mins. Fig. 7a showed the effects of assessing the efficiency of removal of CTSS at constant optimum pH of 2 and varying dosages ranging from 1.0 to 1.8gL^{-1}. The efficiency of removal of the CTSS improved with increased settling time. Throughout the indicated time, the first three dosages (1.0, 1.2, 1.4gL^{-1}) maintained a steady increase in CTSS removal. The dosage of 1.2gL^{-1} with removal efficiency > 87% after 30mins of settling and reported 98.4% removal at the end of 300mins was considered to be optimal dosage. The results of the assessment of CTSS removal at the constant optimum dosage of 1.2gL^{-1} and the varying aqueous solution pH range 2–10 were shown in Fig. 7b. The superiority of the pH value was clearly observed in the CF process. In this investigation the bio-coagulant better performance recorded at acidic pH (especially pH 2) was evident as indicated in Fig. 7b. The figure showed that fair removal efficiency was observed at an alkaline pH of 10 as settling time increased. This is consistent with the literature available (Patrick et al., 2015; Onukwuli et al., 2021).

3.3. Process kinetics

The kinetics of the coagulation-flocculation efficiency of LCS on decontamination of dye-based wastewater using MATLAB 2015b software curve fitting tools have been studied. The kinetic results were obtained at pH 2, with 1.4gL^{-1} of bio-coagulant and an initial dye concentration of 1.0gL^{-1} in the wastewater. The constant of CF rate, K_{11}, of 9.644E-4(L/g.s) , K_R 4.822E-4(L/g.s), $\tau_{1/2}$ 1.1(mins), R^2 0.9655, adjR^2 0.9612, SSE 4.542E-4 and RMSE 7.535E-3 were obtained from the graph of $\frac{1}{\sqrt{N_1}}$, against time based on Eq. (4) and the coagulation time, $\tau_{1/2}$, obtained using Eq. (7). K_{11} is a critical parameter that indicates the CF process output speed and accounts for instant aggregation and subsequent settling. Due to the negligible change in the temperature and viscosity of the dye-based wastewater during the process, K_R, calculated from Eq. (6), showed minimal variance from K_{11}. This matches previous literatures (Okolo et al., 2016). Using statistical parameters, the goodness of fit and adequacy of the experimental data to the primary model as expressed in Eq. (4) was assessed. The R^2 and adjR^2 values are relatively high, and are close to unity. This means the fit to the experimental data is in good agreement. The findings fit previous works (Patrick et al., 2015; Okolo et al., 2016). The SSE and RMSE are very minimal, suggesting minimum fit error and variance from the experimental results, so the fit may be helpful for forecasting.

3.4. Coagulation- adsorption results

To determine the CF adsorption effectiveness of LCS in the CF process, the data obtained from the jar test experiment was used to model the isotherm using Langmuir, Freundlich, and Temkin models, as well as adsorption kinetics using Lagergren pseudo first order and Ho's pseudo second order models for color removal at optimum pH 2.

3.4.1. Adsorption isotherm

Summaries of isotherm parameters, R^2 and adjR^2, SSE and RMSE, were shown in Table 3. The maximum monolayer adsorption capacity (qm) of dye-based wastewater was found

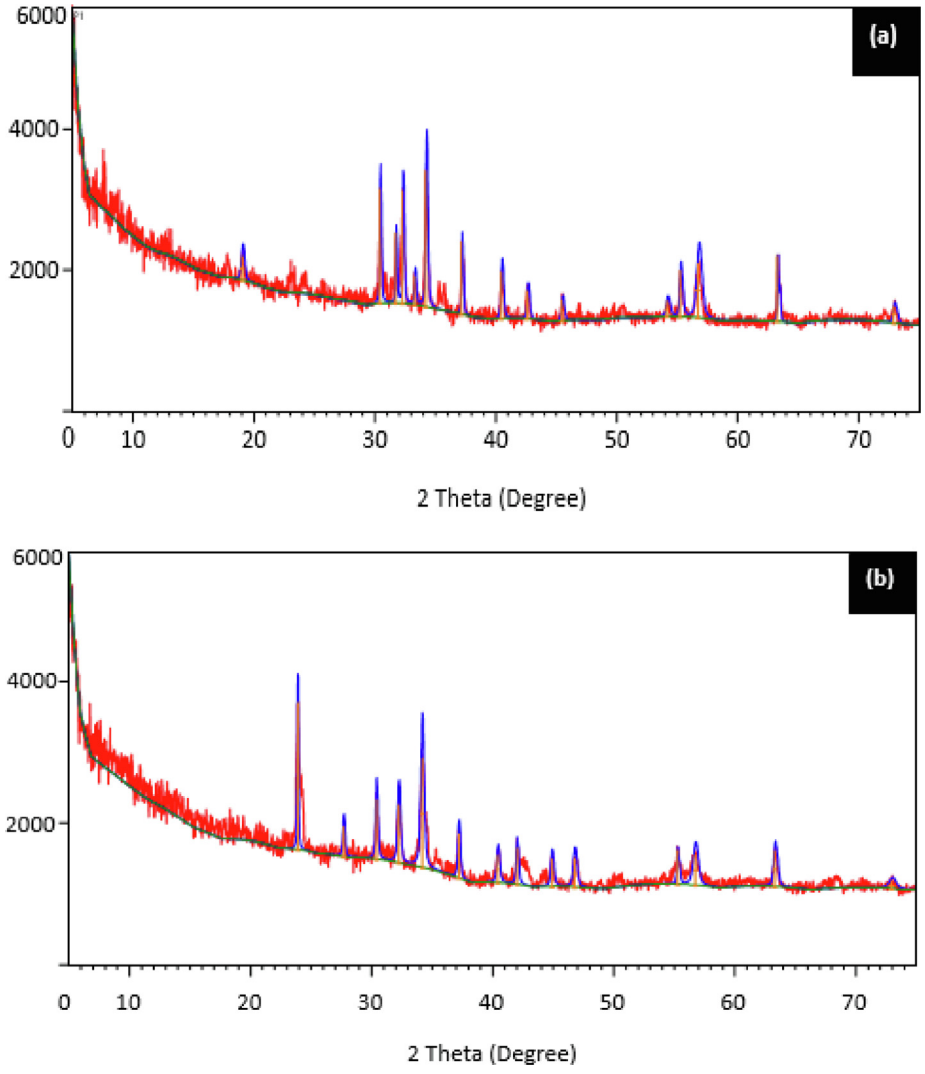

Fig. 5 The XRD spectra of (a) LCS (b) post treatment settled sludge (PTSS).

to be 533.0gg^{-1} by Langmuir, while R^2 was 0.8040. $R_L > 0$ but < 1 is an indicator of favorable dye mixture adsorption on LCS. The value of Freundlich's K_F parameter is 1271.6gg^{-1}(g^{-1})$^{1/n}$. The value of n is 4.819. n > 1 showed a favorable and heterogeneous adsorption value. Also, 4.558e-4 and 148.7 were found to be the values of the Tempkin parameters A and B. The experimental data of these isotherms summarized in Tables 3, shows that compared to the Langmuir and Tempkin models, the Freundlich model provided a better fit with the highest R^2 value. The SSE and RMSE, were also found to be relatively small.

3.4.2. Adsorption kinetic results

Coagulation-flocculation data were applied to the Lagergren's pseudo first and Ho's pseudo second order kinetic models for the adsorption of dye-based wastewater onto biomass and analyzed. The model plots of the adsorption kinetic have been presented, see Fig. 8. Lagergren adsorption constant, K_1 of 0.02439 min^{-1}, adsorption capacity at equilibrium, $q_{e.cal}$ 140gg^{-1}, R^2 0.9449, adjR^2 0.9394, SSE 0.6693 and RMSE 0.2587 were obtained from the log plot (q_e-q_t) against t and the fit tables using linear polynomial in the MATLAB setting, while the $q_{e\cdot exp}$, was 712.1gg^{-1}. The adsorption capacity determined from the fit data at equilibrium, $q_{e\ cal}$, was found not to be similar to the experimental adsorption capacity, $q_{e\ exp}$. The R^2 and adjR^2 were found to be > 0.9, while the SSE and RMSE were moderately low.

Likewise, the pseudo second order model of Ho fitted in Fig. 8b and based on Eq. (14) revealed K_2 1.404e-1 min^{-1}, $q_{e\ cal}$ 821.7gg^{-1}, R^2 0.9771, adjR^2 0.9748, SSE 0.003557 and RMSE 0.01886 were obtained from the t/qt versus t plot and the fit table of the linear polynomial of MATLAB curve fitting tools. The experimental adsorption capacity, $q_{e\ exp}$, was 712.1gg^{-1}. From the results, the equilibrium adsorption capacity, $q_{e\ cal}$, calculated from the fit data, was found to be relatively close to the experimental q_e. It was found that the R^2 and modified R^2 were > 0.9, while the SSE and RMSE were very low. The kinetic data showed that when compared to the first order model, Ho 's second order model was best suited due to high R^2 and its agreement with the experimental values. This is a strong indication that the second order kinetics model was followed by the method. Moreover, relative to the first order model, the SSE and RMSE for the second order were very low. The above confirmed that chemisorption, which

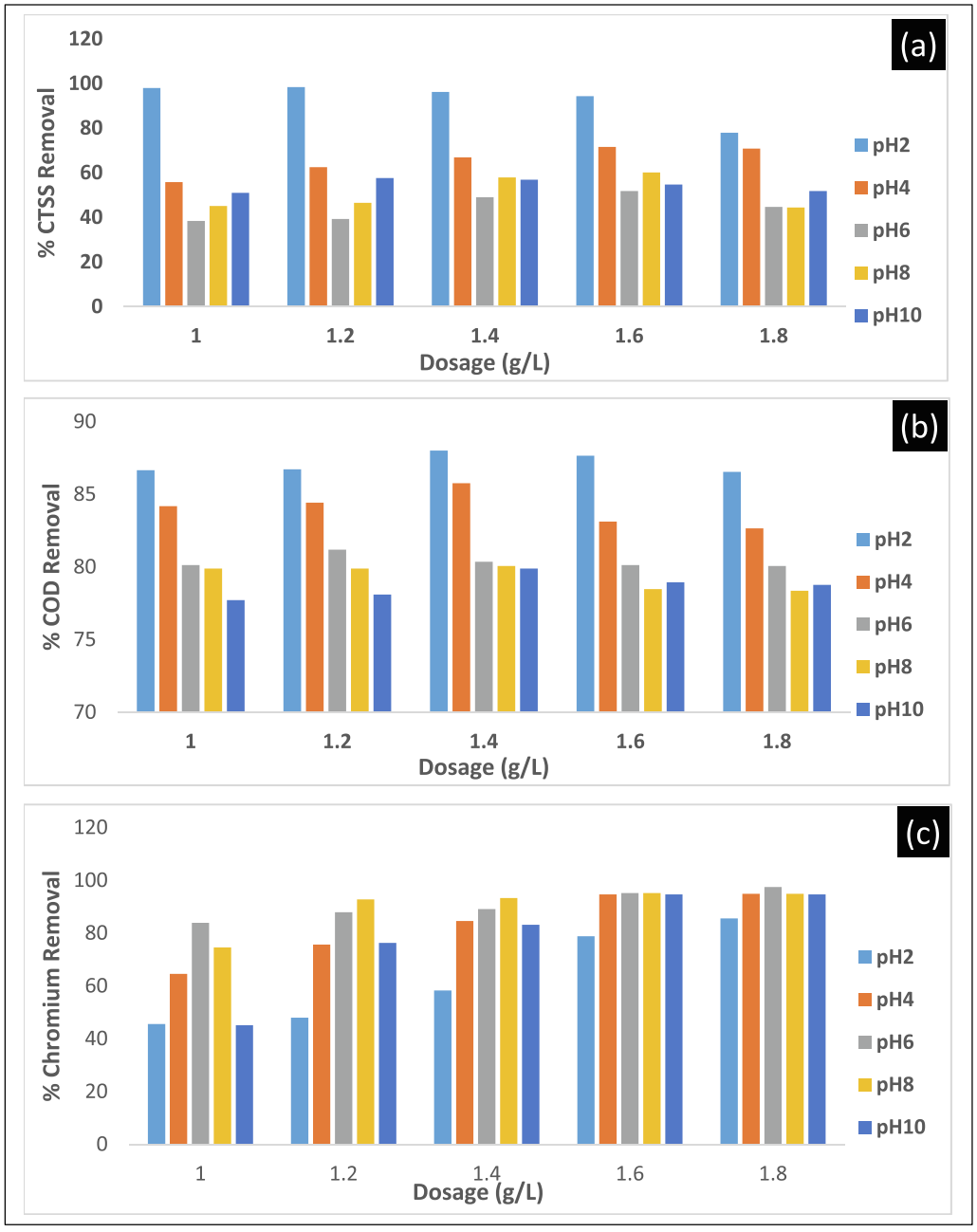

Fig. 6 The plot of dosage and pH effect on the removal efficiency of CTSS(a), COD(b) and Cr (VI)(c) after 300 min settling time.

involves valence forces through electron sharing or exchange, is the rate limiting step.

3.5. Coag-flocculation diffusion (mass transfer) modeling - numerical results

The partial differential equation (model) solution describing the mass transfer rate was resolved using a computational technique (finite differential method). The solutions obtained were programmed and implemented in the MATLAB environment generating various CF profiles. The profiles of CF at different spatial locations are shown in Fig. 9a, while, Fig. 9b demonstrated the correlation at an optimal pH 2.0 and 1.4gL^{-1} between experimental and projected results. As observed in the experimental results, the figure clearly shows the exponential decay pattern, indicating the rate of decrease in dye concentration as the process duration advances. The decrease in dye concentration at the point U (1:301:1) could be attributed to instrumental or human error. The fifth profile of a virtual distribution of particles in Fig. 9a, the experimental results that were obtained and reported in Fig. 9b were similar. These confirm that the model has been adequate for predicting the response variables in the experimental values. This also means that the model is almost in complete harmony with the experimental model, so the model is a critical instrument for the design of the bio-CF system.

R^2, MAD, MSE, RMSE and MAPE were used to further validate the adequacy of the forecast. The findings showed

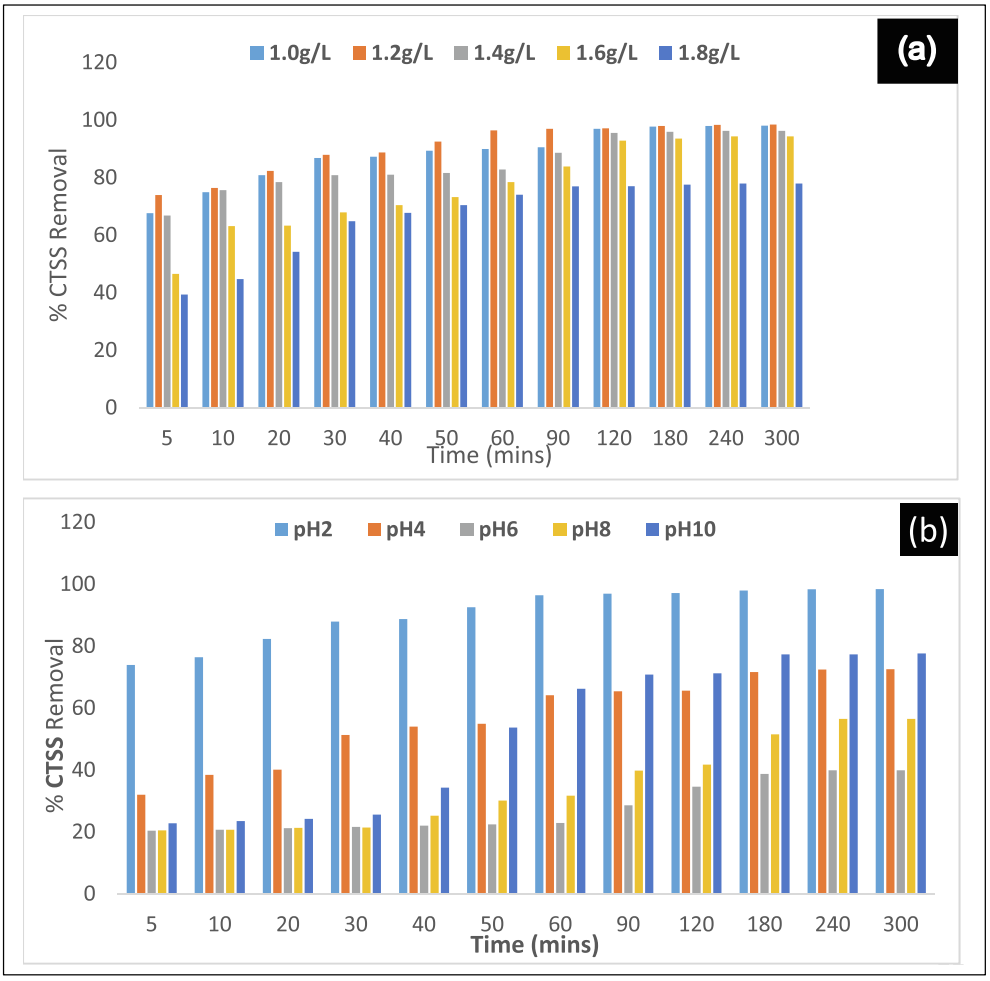

Fig. 7 The plot of settling time effect on the removal efficiency of CTSS at constant pH and varying dosage (a), constant dosage and varying pH (b).

Table 3 Isotherm parameters for CBD/DRD onto LCS at pH 2.

Model/ Parameters	q_m	K_L	R^2	Adj. R^2	SSE	RMSE	R_L
Langmuir Isotherm	533.0	0.1229	0.8040	0.7387	8.527e-8	0.000169	0.8906
Freundlich Isotherm	K_r	N	R^2	Adj. R^2	SSE	RMSE	
	1271.6	4.8190	0.9116	0.8821	0.03473	0.1076	
Temkin Isotherm	A	B	R^2	Adj. R^2	SSE	RMSE	
	4.558e-4	148.7	0.7576	0.6768	3.072e + 4	101.20	

$R^2 > 0.99$ at the optimum dose of 1.4gL^{-1} and pH 2, implying a positive correlation. It was also noted that MAPE 7.50 value were < 10%, showing good model experimental data prediction, and the lower the number, the better the predictive purpose of the model(Jimoda et al., 2013). A close look at the values revealed by MAD, MSE and RMSE; 0.0024, 7.392e-5 and 8.60e-3, respectively, are very small, which is a strong model prediction indicator.

3.6. Response surface fitting by Box-Behnken design (BBD)

Three variables, LCS dosage (X_1), solution pH (X_2) and stirring time (X_3), were correlated with the three responses, Y_1 for CTSS removal (%), Y_2 for COD removal (%) and Y_3 for Cr (VI) removal (%), using a quadratic polynomial equation as provided in Eq. (46). The second order regression mod-

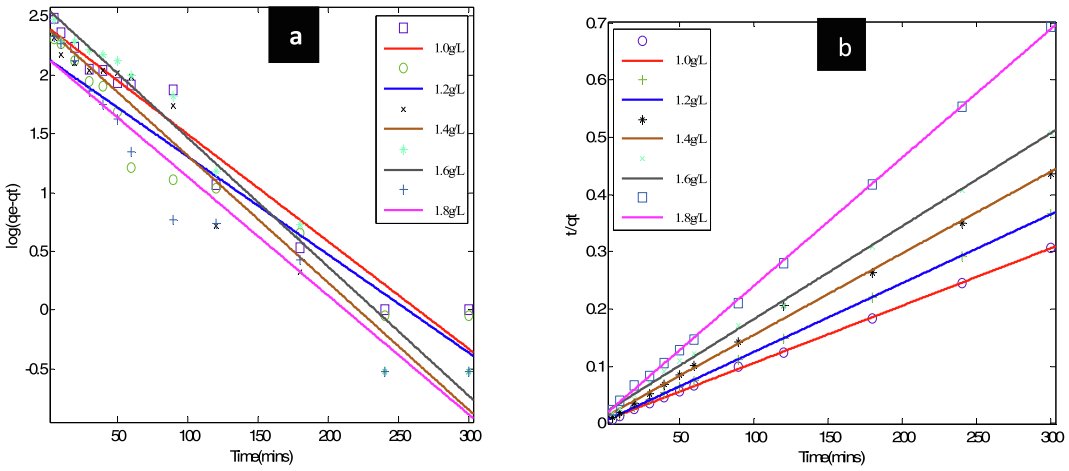

Fig. 8 Adsorption kinetic model plots (a) Lagergren's pseudo first, (b) Ho's pseudo second order.

els were shown in Eqs. (47) - (49), obtained from the experimental results.

$$Y_1 = 47.68 + 6.23X_1 - 35.76X_2 - 7.04X_3 - 2.40X_1X_2 + 2.35X_1X_3 - 9.63X_2X_3 - 28.10{X_1}^2 + 27.67{X_2}^2 - 1.88{X_3}^2 \quad (47)$$

$$Y_2 = 96.80 + 2.50X_1 - 21.49X_2 + 0.18X_3 + 11.47X_1X_2 + 0.19X_1X_3 - 0.17X_2X_3 + 2.99{X_1}^2 - 23.27{X_2}^2 - 2.28{X_3}^2 \quad (48)$$

$$Y_3 = 71.69 + 1.89X_1 + 3.10X_2 + 2.21X_3 + 0.17X_1X_2 + 3.05X_1X_3 - 4.20X_2X_3 + 13.15{X_1}^2 - 34.98{X_2}^2 + 6.71{X_3}^2 \quad (49)$$

Where, respectively, X_1, X_2 and X_3 were LCS dosage, solution pH and stirring time. The effect of a single variable is defined by the coefficient of one factor, while the interaction between the two variables and the quadratic effect is defined by the coefficient of two factors and those with a second order term. A positive sign before the words indicates a synergistic effect, while a negative sign indicates an antagonistic effect (Kim, 2016). Following the elimination, as shown in Table 4, of non-significant terms, Eqs. (50) - (52) imaged.

$$Y_1 = 47.68 + 6.23X_1 - 35.76X_2 - 9.63X_2X_3 - 28.10{X_1}^2 + 27.67{X_2}^2 \quad (50)$$

$$Y_2 = 96.80 + 2.50X_1 - 21.49X_2 + 11.47X_1X_2 - 23.27{X_2}^2 \quad (51)$$

$$Y_3 = 71.69 + 3.1X_2 + 2.21X_3 + 3.05X_1X_3 - 4.2X_2X_3 + 13.15{X_1}^2 - 34.98{X_2}^2 + 6.71{X_3}^2 \quad (52)$$

3.6.1. Model adequacy

To assess the adequacy of the models, model overview statistics and ANOVA were used. While the ANOVA was presented in Table 4, the model overview statistics revealed R^2 0.8293 and adjR^2 0.6099, R^2 0.9584 and adjR^2 0.9050, and R^2 0.9935, adjR^2 0.9851, for CTSS, COD and Cr (VI) removal responses, respectively. The p-value for CTSS removal from the ANOVA table was 0.0467, while that of COD and Cr (VI) removal were < 0.01 for the model chosen. For CTSS, COD and Cr (VI) removal, the model summary statistics showing R^2, of 0.8293, 0.9584 and 0.9935, respectively, suggested that the empirical model could not explain only 17.07%, 4.16% and 0.65% of the variance. The high R^2 values suggested that the model was well suited to the response (Okolo et al., 2018). It can also be seen from the findings that the experiment indicates a desirable and rational alignment with the R^2 's proximity to the adjR^2. This closeness ensures that the quadratic models are satisfactorily adapted to the experimental data (Okolo et al., 2018).

The second order regression for the efficiency of CTSS, COD and Cr (VI) removal indicate that the models were significant because the f-values of 3.78, 17.6 and 118.56, respectively, were high. Similarly, for quadratic regression models, the p-value that gives an indicator of the importance of a model in relation to the f-value was < 0.05. For a 95% confidence level, this showed that the models were statistically significant, indicating only a 5% risk that the f-value was due to noise. The model is not significant if the p-value is above 0.1(Okolo et al., 2018).

3.6.2. Process analysis

Table 4 also, explains the linear (X_1, X_2, X_3), quadratic (X_1^2, X_2^2, X_3^2) and interaction (X_1X_2, X_2X_3, X_1X_3) effects of the parameters. From the table, the response, Y_1, revealed that X_1, X_2, X_1^2, X_2^2, and X_2X_3 are significant terms with $p < 0.05$, while X_3, X_3^2, X_2X_3 and X_1X_3 are not significant terms. Similarly, Y_2 response have significant terms of X_1, X_2, X_2^2, X_1X_2, while X_3, X_1^2, X_3^2, X_1X_3, X_2X_3 are not significant. Also, from the table, the response, Y_3, shows that X_2, X_3, X_1X_3, X_2X_3, X_1^2, X_2^2 and X_3^2 are all significant terms. Only X_1 and X_1X_2 are not significant. The lack of fit f-values of 1.62, 5.60 and 5.10 for Y_1, Y_2 and Y_3, respectively, imply that the lack of fit is not significant relative to the pure error. There are only 13.770%, 28.97% and 7.48% for Y_1, Y_2 and Y_3, respectively, chance that the lack of fit f-values this large could

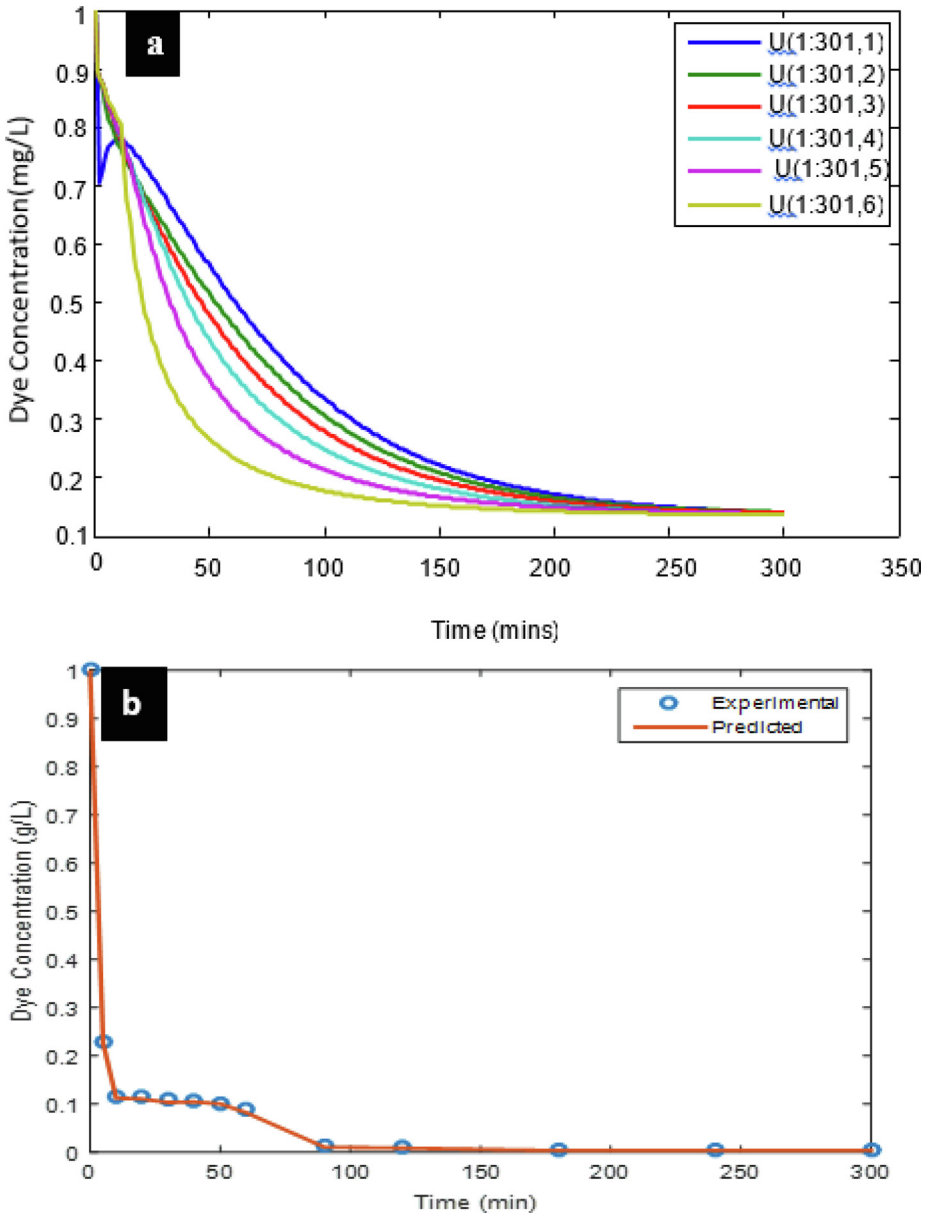

Fig. 9 Dye concentration distribution simulation at varying spatial position (a), simulated and experimental dye concentration over time (b) at pH2 and 1.4gL$^{-1.}$

occur due to noise. Non-significant lack of fit is good, the model needs to fit.

3.6.3. Effect of variables on CTSS, Cr (VI) and COD removal efficiency

The 3-D response surface plots in Fig. 10 showed the individual and combined effect of LCS dosage, solution pH and stirring time on the percent CTSS, COD and Cr (VI) removal based on a total of 17 BB-design of the three variables. The surface graph which is a representative of the model used to visualize the relationship between the response and the experimental data showed curvilinear profiles and significant curvatures. The distinct curves for the relationship between pH and dosage, pH and stirring time, dosage and stirring time variables, clearly depict their interactions in the process This is consistent with the quadratic model and an indication that the independent variables have strong interactions(Imen et al., 2013). Optimum condition at 1.4gL^{-1} dosage, pH 2 and 30mins stirring were indicated by the response surface plots, giving 99.20% CTSS removal, with 1.4gL^{-1} dosage, pH 2 at 30mins stirring, giving 90.07% COD removal and at 1.8 g/L dosage, pH6 and 15mins giving 98.29% Cr (VI) removal, respectively.

3.6.4. Validation of the optimized parameters of the coagulation process based on RSM

The optimized results were validated experimentally by carry-out triplicate experiment and the average treatment efficiencies obtained are shown in Table 5. It can be shown in Table 5 that the optimum experimental validated % removal efficiency of

Table 4 ANOVA results for three responses.

Response	Source	SS	DF	MS	F-value	Prob > F	Remark
Y_1(CTSS) %	Model	17591.0	9	1954.6	3.78	0.0467	Suggested
Linear	X_1	210.01	1	210.01	4.60	0.0464	
	X_2	10231.7	1	10231.6	19.78	0.0030	
	X_3	396.21	1	396.21	0.77	0.4105	
Pure quadratic	X_1^2	3325.27	1	3325.27	6.43	0.0389	
	X_2^2	3224.28	1	3224.28	6.23	0.0412	
	X_3^2	14.84	1	14.84	0.029	0.8703	
Interaction	X_1 X_2	123.04	1	123.04	3.045	0.0838	
	X_1 X_3	370.56	1	370.56	2.72	0.0425	
	X_2 X_3	22.09	1	22.09	0.043	0.8422	
	Residual	3620.41	7	517.20			
	Lack of fit	1150.18	3	383.39	1.62	0.1377	Not significant
	Pure error	2470.23	4	617.56			
	Cor. Total	21211.4	16				
Y_2(COD) %	Model	188.06	9	20.90	17.60	0.0005	Suggested
Linear	X_1	0.30	1	0.30	11.18	0.03107	
	X_2	112.65	1	112.65	87.5	< 0.0001	
	X_3	0.042	1	0.042	0.18	0.9412	
Pure quadratic	X_1^2	2.62	1	2.62	0.89	0.3758	
	X_2^2	0.14	1	0.14	58.57	0.0001	
	X_3^2	5.52	1	5.52	0.52	0.4951	
Interaction	X_1 X_2	0.15	1	0.15	12.61	0.0096	
	X_1 X_3	60.93	1	60.93	5.42	0.0961	
	X_2 X_3	3.99	1	3.99	0.75	0.9550	
	Residual	1.67	7	0.24			
	Lack of fit	1.10	3	0.37	5.60	0.2897	Not significant
	Pure error	0.57	4	0.14			
	Cor. Total	189.73	16				
Y_3(Cr (VI)) %	Model	6071.81	9	674.65	118.56	< 0.0001	Suggested
Linear	X_1	28.58	1	28.58	5.02	0.0600	
	X_2	77.00	1	77.00	13.53	0.0079	
	X_3	39.16	1	39.16	6.88	0.0342	
Pure quadratic	X_1^2	728.54	1	728.54	128.03	< 0.0001	
	X_2^2	5150.82	1	5150.82	905.17	< 0.0001	
	X_3^2	189.52	1	189.52	33.30	0.0007	
Interaction	X_1 X_2	0.12	1	0.12	0.020	0.8907	
	X_1 X_3	37.21	1	37.21	6.54	0.0377	
	X_2 X_3	70.56	1	70.56	12.40	0.0097	
	Residual	39.83	7	5.69			
	Lack of fit	31.57	3	10.52	5.10	0.0748	Not significant
	Pure error	8.26	4	2.06			
	Cor. Total	6111.64	16				

CTSS, COD and Cr (VI) are close to the model predicted values at the same optimum conditions.

4. Conclusion

In this research, coag-flocculation method was used to evaluate the efficiency of LCS as an effective biomass for the decontamination of dye-based wastewater at the condition of the analysis. LCS features suggested coagulant with sufficiently active site to be used as a bio-coagulant. The composition of the sludge obtained suggests that it may be a resource for wastewater-absorbed materials. The coag-flocculation system using LCS efficiently extracted 99.2% CTSS at wastewater pH 2 with 1400mgL^{-1}; 90.07% of COD with 1400mgL^{-1} and wastewater pH 2 and 98.29% of chromium (VI) with 1800mgL^{-1} and wastewater pH 6. In addition, the study revealed that LCS dosage and wastewater pH had a major influence on the results. The kinetic, mass transfer, optimization and CF adsorptive parameters were also obtained. The indicators of error were very minimal. The kinetic and mass transfer simulation results predicted were in agreement with the experimental results. Therefore, the use of LCS has adequately demonstrated the potential of a bio-coagulant alternative in the treatment of dye-based wastewater. The kinetic, mass transfer, optimization and CF adsorptive data obtained could be useful for design, start-up operating time, design control and optimization of the process of bio-coagulation.

Declaration of Competing Interest

The authors declare that they have no known competing financial interests or personal relationships that could have appeared to influence the work reported in this paper.

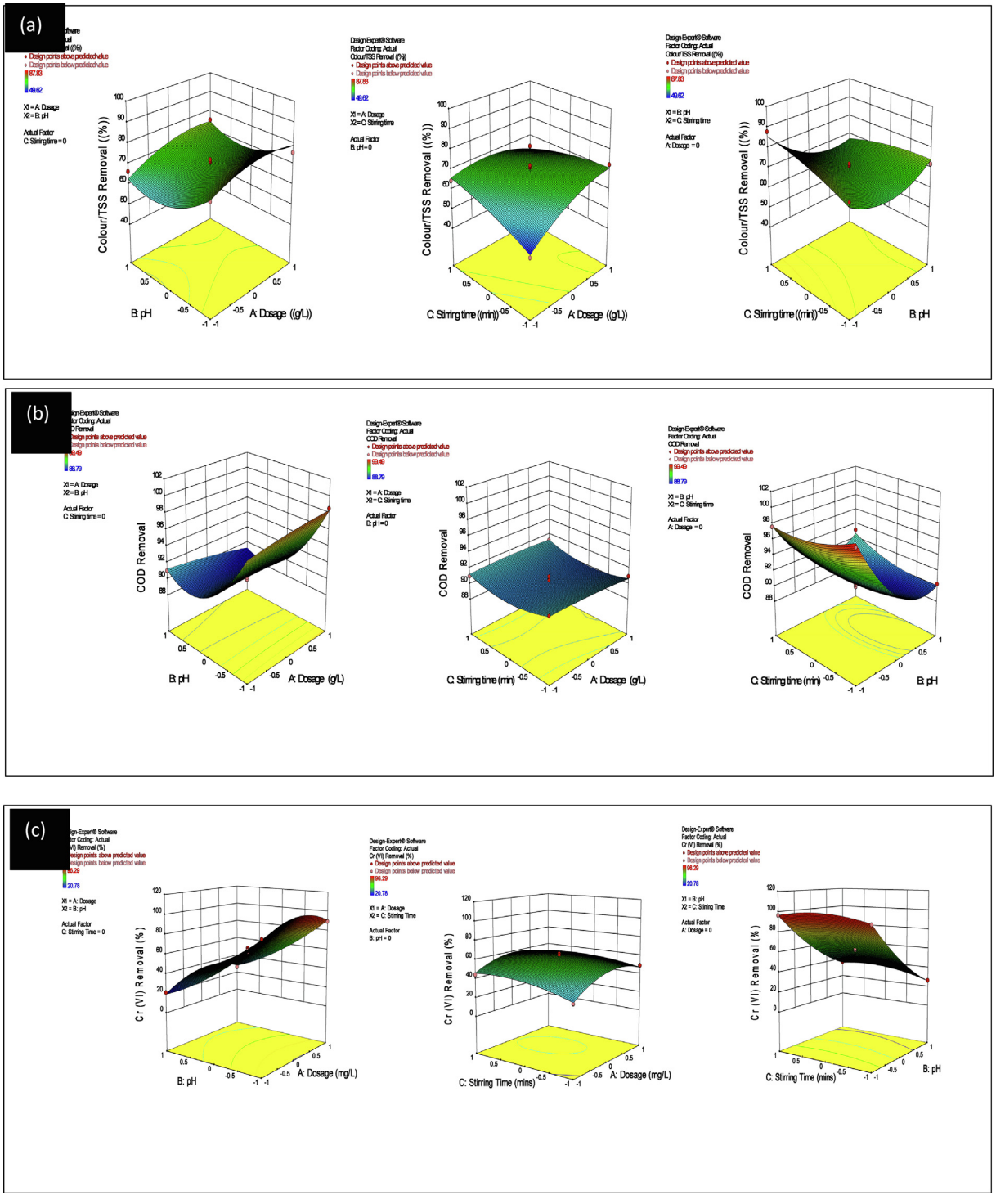

Fig. 10 3-D response surface plots for CTSS (a), COD (b) and Cr (VI) (c) removal efficiency.

Table 5 Process variables that gave the optimum results.

Variables	Dosage (g/L)	pH	Time (mins)	BBD Optimized Results (%)	Experimental Validated result (%)
CTSS	1.4	2	30	99.20	98.9
COD	1.4	2	30	90.07	89.6
Cr (VI)	1.8	2	30	98.29	96.8

Acknowledgement

P.C. Nnaji and I.G. Ezemagu are grateful to Department of Chemical Engineering, Michael Okpara University, Umudike and Department of Chemical Engineering, Nnamdi Azikiwe University, Nigeria. V.C. Anadebe is grateful to CSIR, India and TWAS Italy for the Postgraduate Fellowship (Award No. 22/FF/CSIR-TWAS/2019) to purse research programme in CSIR-CECRI, India. In addition, Alex Ekwueme Federal University Ndufu-Alike Ebonyi State, Nigeria, is acknowledged for the Research Leave to visit CECRI, India

References

Ahmad, R., Haseeb, S., 2015. Competitive adsorption of Cu2+ and Ni2+ on Luffa acutangula modified Tetraethoxysilane (LAP-TS) from the aqueous solution: Thermodynamic and isotherm studies. Groundwater Sustainable Dev. 1 (1–2), 146–154.

Ahmadi, M., Ghanbari, F., Madihi-bidgoli, S., 2016. Journal of Photochemistry and Photobiology A : Chemistry Photoperoxi-coagulation using activated carbon fi ber cathode as an ef fi cient method for benzotriazole removal from aqueous solutions : Modeling, optimization and mechanism. J. Photochemistry Photobiology, A: Chem. 322–323, 85–94.

Akpomie, K.G., Conradie, J., 2021. Ultrasonic aided sorption of oil from oil-in-water emulsion onto oleophilic natural organic-silver nanocomposite. Chem. Eng. Res. Des. 165, 12–24.

Alves, D.C.S., Coseglio, B.B., Pinto, L.A.A., Cadaval, T.R.S., 2020. Development of Spirulina/chitosan foam adsorbent for phenol adsorption. J. Mol. Liq. 309, 113256.

Anastopoulos, I., Pashalidis, I., 2020. Environmental applications of Luffa cylindrica-based adsorbents. J. Mol. Liq. 319, 114127.

Ani, J.U., Nnaji, N.J.N., Onukwuli, O.D., Okoye, C.O.B., 2012. Nephelometric and functional parameters response of coagulation for the purification of industrial wastewater using Detarium microcarpum. J. Hazard. Mater. 243, 59–66.

Aoac, 2005. Official Methods of Analysis. Association of Official Analytical Chemist, Gaitherburg.

AWWA, APHA, WEF, 2012. Standard Method for the Examination of Water and Wastewater, 22nd Edition, New York.

Baharlouei, A., Jalilnejad, E., Sirousazar, M., 2018. Fixed-bed column performance of methylene blue biosorption by Luffa cylindrica: statistical and mathematical modeling. Chem. Eng. Commun. 205 (11), 1537–1554.

Dalvand, A., Gholibegloo, E., Ganjali, M.R., Golchinpoor, N., Khazaei, M., Kamani, H., Mahvi, A.H., 2016. Comparison of Moringa stenopetala seed extract as a clean coagulant with Alum and Moringa stenopetala-Alum hybrid coagulant to remove direct dye from Textile Wastewater. Environ. Sci. Pollut. Res. 23 (16), 16396–16405.

de Souza, M. T. F., de Almeida, C. A., Ambrosio, E., Santos, L. B., Freitas, T. K. F. de S., Manholer, D. D., … Garcia, J. C. (2016). Extraction and use of Cereus peruvianus cactus mucilage in the treatment of textile effluents. *J. Taiwan Inst. Chem. Eng.*, *67*, 174–183.

Ejimofor, M., Ezemagu, I.G., Menkiti, M.C., 2021a. RSM and ANN-GA modeling of colloidal particles removal from paint wastewater via coagulation method using modified Aguleri montmorillonite clay. Current Res. Green Sustainable Chem. 4, 100164.

Ejimofor, M., Menkiti, M., Ezemagu, I., 2021b. Integrated Treatment of Paint Wastewater Using Helix Pometia Shell Coagulant and Sludge Conversion to Biogas: Process Thermodynamics and Biogas Energy Content. Int. J. Plant, Animal Environ. Sci. 11 (03), 391–422.

Ezemagu, I.G., Ejimofor, M.I., Menkiti, M.C., Nwobi-Okoye, C.C., 2021a. Modeling and optimization of turbidity removal from produced water using response surface methodology and artificial neural network. S. Afr. J. Chem. Eng. 35, 78–88.

Ezemagu, I.G., Ejimofor, M.I., Menkiti, M.C., 2021b. Instrumental and thermal characterization of the sludge generated after bio-coagulation treatment (GSABT) of petroleum produced water (PW). Results Eng. 9, 100187.

Ezemagu, I.G., Ejimofor, M.I., Menkiti, M.C., Diyoke, C., 2021c. Biofertilizer production via composting of digestate obtained from anaerobic digestion of post biocoagulation sludge blended with saw dust: Physiochemical characterization and kinetic study. Environ. Challenges 5, 100288.

Ezemagu, I.G., Ejimofor, M.I., Menkiti, M.C., 2020. Turbidimetric study for the decontamination of paint effluent (PE) using mucuna seed coagulant (MSC): Statistical design and coag-flocculation modelling Turbidimetric study for the decontamination of paint effluent (PE) using mucuna seed coagulant. Environ. Adv. 2, 100023.

Ezemagu, I.G., Menkiti, M.C., Ugonabo, V.I., Aneke, M.C., 2016. Adsorptive approach on nepholometric study of paint effluent using Tympanotonos fuscatus extract. Bull. Chem. Soc. Ethiop. 30 (3), 377–390.

Hadi, S.M., Al-Mashhadani, M.K.H., Eisa, M.Y., 2019. Optimization of dye adsorption process for Albizia lebbeck pods as a biomass using central composite rotatable design model. Chem. Industry Chem. Eng. Quarterly 25 (1), 39–46.

Howe, K.J., Hand, D.W., Crittenden, J.C., Trussell, R.R., Tchobanoglous, G., 2012. Principles of Water Treatment. John Wiley and Sons Inc., pp. 139–142.

Imen, F., Lamia, K., Asma, T., Neacute ji, G., & Radhouane, G. (2013). Optimization of coagulation-flocculation process for printing ink industrial wastewater treatment using response surface methodology. *African J. Biotechnol.*, *12*(30), 4819–4826.

Irfan, M., Butt, T., Imtiaz, N., Abbas, N., Ahmad, R., Shafique, A., 2017. The removal of COD, TSS and colour of black liquor by coagulation – flocculation process at optimized pH, settling and dosing rate. Arabian J. Chem. 10, S2307–S2318.

Jadhav, M.V., Mahajan, Y.S., 2014. Assessment of feasibility of natural coagulants in turbidity removal and modeling of coagulation process. Desalin. Water Treat. 52 (31–33), 5812–5821.

Jafari, F., Nasirizadeh, N., Mirjalili, M., 2020. Enhanced degradation of reactive dyes using a novel carbon ceramic electrode based on copper nanoparticles and multiwall carbon nanotubes. Chin. J. Chem. Eng. 28 (1), 318–327.

Jiang, X., Sun, P., Xu, L., Xue, Y., Zhang, H., Zhu, W., 2020. Platanus orientalis leaves based hierarchical porous carbon microspheres as high efficiency adsorbents for organic dyes removal. Chin. J. Chem. Eng. 28 (1), 254–265.

Jimoda, L., 2013. Modelling of Mass Transfer Rate During Biocoagulation-Flocculation of Coal-Rich Wastewater. J. Sci. Res. Rep. 2 (1), 376–390.

Jorfi, S., Alavi, S., Jaafarzadeh, N., Ghanbari, F., Ahmadi, M., 2018. COD removal from high salinity petrochemical wastewater using Photo-assisted peroxi-coagulation. Chem. Biochem. Eng. Q. 32 (2), 229–238.

Joshi, S., Bajpai, S., Jana, S., 2020. Application of ANN and RSM on fluoride removal using chemically activated D. sissoo sawdust. Environ. Sci. Pollut. Res. 27 (15), 17717–17729.

Kim, S.C., 2016. Application of response surface method as an experimental design to optimize coagulation-flocculation process for pre-treating paper wastewater. J. Ind. Eng. Chem. 38, 93–102.

Li, Z., Jiang, L., Tang, C., 2020. Investigation on removing recalcitrant toxic organic polluters in coking wastewater by forward osmosis. Chin. J. Chem. Eng. 28 (1), 122–135.

Menkiti, M., Anaehobi, H., Nnaji, P., 2015. Process Optimization and Kinetics of Biolubricant Synthesis From Fluted Pumpkin Seed. European Sci. J. 11 (27), 30–47.

Menkiti, M.C., Okoani, A.O., Ejimofor, M.I., 2018a. Adsorptive study of coagulation treatment of paint wastewater using novel Brachystegia eurycoma extract. Appl. Water Sci. 8 (6), 1–15.

Menkiti, M., Ezemagu, I., Okolo, B., 2016. Perikinetics and sludge study for the decontamination of petroleum produced water (PW) using novel mucuna seed extract Collision factor for Brownian transport. Pet. Sci. 13 (2), 328–339.

Menkiti, M., Ezemagu, I., Singaraju, S., 2018b. Focus on adsorptive equilibrium, kinetics and thermodynamic components of petroleum produced water biocoagulation using novel Tympanotonos Fuscatus extract. Petroleum 4 (1), 56–64.

Menkiti, M.C., Onukwuli, O.D., 2011. Single and multi angle nephelometric approach to the study of coag-flocculation of coal effluent medium using Brachystegia eurycoma coagulant (BEC) 8 (1), 61–76.

Menkiti, M.C., Ezemagu, I.G., 2015. Sludge characterization and treatment of produced water(PW) using Tympanotonos Fuscatus coagulant (TFC). Petroleum 1 (1), 51–62.

Nandiyanto, A.B.D., Oktiani, R., Ragadhita, R., 2019. How to read and interpret ftir spectroscope of organic material. Indonesian J. Sci. Technology 4 (1), 97–118.

Nnaji, P., Anadebe, C., Onukwuli, O.D., 2020a. Application of experimental design methodology to optimize dye removal by mucuna sloanei induced coagulation of dye-based wastewater. Desalin. Water Treat. 198, 396–406.

Nnaji, P.C., Okolo, B.I., Menkiti, M.C., 2014. Nephelometric Performance Evaluation of Oxidized Starch in the Treatment of Coal Washery Effluent. Natural Resources 05 (03), 79–89.

Nnaji, P.C., Okolo, B.I., Onukwuli, O.D., 2020b. Luffa cylindrica seed: Biomass for wastewater treament, sludge generation study at optimum conditions. Chem. Industry Chem. Eng. Quarterly 26 (4), 349–358.

Nnaji, P.C., Okoye, C.C., Umeuzuegbu, J.U., 2020c. Efficiency evaluation of Luffa cylindrica and Mucuna sloanei seeds in dye removal : A news approach. Int. Sci. J. 146 (June), 184–201.

Okolo, B.I., Nnaji, P.C., Oke, E.O., Adekunle, K.F., Ume, C.S., Onukwuli, O.D., 2018. Optimizing bio-coagulants for brewery wastewater treatment using response surface methodology. Nigerian J. Technology 36 (4), 1104.

Okolo, B.I., Nnaji, P.C., Onukwuli, O.D., 2016. Nephelometric approach to study coagulation-flocculation of brewery effluent medium using Detarium microcarpum seed powder by response surface methodology. J. Environ. Chem. Eng. 4, 992–1001.

Onukwuli, O.D., Nnaji, P.C., Menkiti, M.C., Anadebe, V.C., Oke, E. O., Ude, C.N., Okafor, N.A., 2021. Dual-purpose optimization of dye-polluted wastewater decontamination using bio-coagulants from multiple processing techniques via neural intelligence algorithm and response surface methodology. J. Taiwan Inst. Chem. Eng. 125, 372–386.

Patrick, C., Bernard, I., Chukwudi, M., Sunday, U., Agu, C., 2015. Kinetics and Particle Removal Profile of Pulverized Snail Shell – Alum Induced Coag-Flocculation of Quarry Effluent. British J. Appl. Sci. Technol. 5 (6), 621–632.

Prabhu, P.R., Prabhu, D., Rao, P., 2020. Analysis of Garcinia indica Choisy extract as eco-friendly corrosion inhibitor for aluminum in phosphoric acid using the design of experiment. Integrative Medicine Res. 9 (3), 3622–3631.

Stroud, 1987. Engineering Mathematics, Programme and Problem. Macmillan Education Ltd, 448.

Shahidi, A., Jalilnejad, N., & Jalilnejad, E. (n.d.). A study on adsorption of cadmium (II) ions from aqueous solution using Luffa cylindrica. *Desalination and Water Treatment,* (May 2015), 37–41.

Wang, A., Zheng, Z., Li, R., Hu, D., Lu, Y., Luo, H., Yan, K., 2019. Biomass-derived porous carbon highly efficient for removal of Pb (II) and Cd(II). Green Energy Environ. 4 (4), 414–423.

Zhao, B., Xiao, W., Shang, Y., Zhu, H., Han, R., 2017. Adsorption of light green anionic dye using cationic surfactant-modified peanut husk in batch mode. Arabian J. Chem. 10, S3595–S3602.